Journal of Materials Chemistry A

# Graphene oxide supported sodium stannate lithium ion battery anodes by the peroxide route: Low temperature and no waste processing



| | |
|---|---|
| Journal: | *Journal of Materials Chemistry A* |
| Manuscript ID: | TA-ART-06-2015-004514.R1 |
| Article Type: | Paper |
| Date Submitted by the Author: | 17-Aug-2015 |





| | |
|---|---|
| Complete List of Authors: | Mikhaylov, Alexey; Kurnakov Institute of General and Inorganic Chemistry, Russian Academy of Sciences, ; The Casali Institute and the Institute of Chemistry, The Hebrew University of Jerusalem,<br>Medvedev, Alexander; Institute of General and Inorganic Chemistry RAS, ; THE HEBREW UNIVERSITY, The Casali Center The Chemistry Institute<br>Mason, Chad; TUM CREATE, Electrochemistry & New Materials<br>Nagasubramanian, Arun; TUM CREATE, Electrochemistry & New Materials, ; Energy Research Institute @ NTU, ; NTU, materials science and engineering,<br>Srinivasan, Madhavi; TUM CREATE, Electrochemistry & New Materials, ; Energy Research Institute @ NTU, ; Nanyang Technological University, Materials Science and Engineering<br>Batabyal, Sudip; Energy Research Institute @ NTU,<br>Zhang, qichun; NTU, materials science and engineering<br>Gun, Jenny; The Casali Institute and the Institute of Chemistry, The Hebrew University of Jerusalem,<br>Prikhodchenko, Petr; Energy Research Institute @ NTU,<br>Lev, Ovadia; School of Applied Science and Technology, Division of Environmental Sciences |

Journal Name

ARTICLE

# Graphene oxide supported sodium stannate lithium ion battery anodes by the peroxide route: Low temperature and no waste processing

Received 00th January 20xx,
Accepted 00th January 20xx

DOI: 10.1039/x0xx00000x

www.rsc.org/

A. A. Mikhaylov,[a,b] A. G. Medvedev,[a,b] C. W. Mason,[c] A. Nagasubramanian, [c,d,e] S. Madhavi, [c,d,e] S. K. Batabyal,[d] Q. Zhang,[e] J. Gun,[b] P. V. Prikhodchenko*[a,d] and O. Lev*[b]

With the large performance improvement of graphene supported tin based lithium ion battery anodes they became a viable alternative to the state of the art graphite anodes. However, currently these anodes are produced by energy demanding thermal processes and generate lithium chloride or other wastes. In this research we demonstrate the formation of efficient and stable lithium ion battery anode based on sodium stannate coated reduced graphene oxide. Coating is performed at low temperature, and when sodium peroxostannate precursor is used, the process can be made with zero waste discharge. Thermal treatment is required only for the solid material. The anode exhibited charge capacity of 610 mAh $g^{-1}$ after 140 cycles at 100 mA $g^{-1}$. This is the first characterization of the sodium stannate based anode for LIB.

## Introduction

Tin oxide based electrodes are a well-known alternative to graphite for high-energy applications. Tin is non-toxic, relatively abundant, and of low cost. $SnO_2$ exhibits lithium alloying with the Sn phase which provides 783 mAh $g^{-1,}$ and additional 707 mAh $g^{-1}$ can be obtained when the slower process of tin oxide formation can be reversibly exploited (Equations 1, 2).

$$SnO_2 + 4Li^+ + 4e^- \rightarrow Sn + 2Li_2O \quad (1)$$

$$Sn + 4.4Li^+ + 4.4e^- \leftrightarrow Li_{4.4}Sn \quad (2)$$

These values are four times higher compared to the capacity of graphite anode, 372 mAh $g^{-1}$, though the lithium oxide exploitation involves larger potentials and lower power density.[1] Reduced graphene oxide, rGO - tin oxide composites are especially attractive since rGO is conductive and can thus distribute the charge efficiently by decreasing the diffusional pathway between the electrolyte and the current collector.

Volume changes due to lithiation can reach 240 % for a 4.4 Li:Sn stoichiometry[2] and 300 % volume expansion can be obtained for the 8.4 stoichiometry.[3] Repeated volume changes due to charge/ discharge cycling pulverizes the active anode material and decreases its electric connectivity. Two approaches are commonly used to prevent pulverization. Nanograins of host material accommodate stress and strain, and flexible carbon support maintains electronic conductivity. A few layers graphene oxide platelets are flexible enough to buffer the large volume change due to lithium alloying.

Table 1 compiles recent reports of exceptionally high-performance graphene – tin oxide composites and shows that in the last couple of years, exceedingly high specific charge capacities could be obtained. At times, the anode capacity exceeds 1400 mAh $g^{-1}$,[4,5] approaching and even exceeding the theoretical, 8.4 Li:Sn stoichiometry. This seems incredibly advantageous at first sight, though since the specific capacity of the lithium ion battery cathodes remains lower (about 200-300 mAh $g^{-1}$) in a practical two electrode cell the cathodes is much heavier than the anode, and thus the additional gain in weight of the two electrodes is less important for the high efficiency end. The gain obtained by a fourfold increase of the capacity of the anode (to 1488 mAh $g^{-1}$) compared to the 372 mAh $g^{-1}$ of the graphite is only 33 % compared to 22 % gain that is obtained by doubling the charge capacity of the anode to 744 mAh $g^{-1}$. Furthermore, the very low voltage of graphite (~ 0.1V vs. $Li/Li^+$) helps it retain energy density competitiveness versus higher voltage alternatives. Thus, as the anode efficiencies become higher, there is a decreasing incentive to further increase the anode charging capacity, and economic and sustainable electrode manufacturing becomes more important.[6] Column 2 of Table 1 illuminates another aspect of tin oxide composites. In most cases, the electrode processing

[a] Kurnakov Institute of General and Inorganic Chemistry, Russian Academy of Sciences, Leninskii prosp.31,Moscow 119991, Russia. prikhman@gmail.com
[b] The Casali Center of Applied Chemistry, The Institute of Chemistry, The Hebrew University of Jerusalem, Jerusalem 91904, Israel. ovadia@mail.huji.ac.il
[c] TUM CREATE, 1 CREATE Way, 10-02 Create Tower, Singapore 138602, Singapore.
[d] Energy Research Institute @ NTU, Nanyang Technological University, 50 Nanyang Avenue, Singapore 639798, Singapore.
[e] School of Materials Science and Engineering, Nanyang Technological University 50 Nanyang Avenue, Singapore 639798, Singapore.

Electronic Supplementary Information (ESI) available: Thermal analysis of GO supported sodium peroxostannate, XRD data of NaSnOx-GO500-2, charge capacity of the NaSnOx-GO400 anodes upon repeated cycling, microscopies, spectroscopies and XRD equipments used for materials characterization. See DOI: 10.1039/x0xx00000x

Table 1: Recently reported highly efficient tin oxide – graphene composite lithium ion battery anodes: Performance and processing conditions.

| Formation process | Precursor | Capacity, mAh $g^{-1}$ | Cycles | Reference |
|---|---|---|---|---|
| Hydrothermal | $SnCl_4$ | 703 | 80 | [8] |
| | | 1000 | 400 | [9] |
| | | 756 | 50 | [10] |
| | | 801 | 50 | [11] |
| | | 996 | 100 | [12] |
| | | 1198 | 115 | [13] |
| | | 794 | 20 | [14] |
| | | 1244 | 50 | [15] |
| | | 1305 | 500 | [3] |
| | | 892 | 20 | [16] |
| | | 710 | 50 | [17] |
| | | 847 | 50 | [18] |
| | | 1346 | 500 | [19] |
| | | 1100 | 100 | [20] |
| | | 808 (1290) | 100 | [21] |
| | $SnCl_2$ | 985 | 30 | [22] |
| | | 1546 | 40 | [4] |
| | | 794 | 50 | [23] |
| | | 1027 | 165 | [24] |
| | | 825 | 50 | [25] |
| | | 890 | 500 | [26] |
| | | 1220 | 100 | [27] |
| | | 1419 | 150 | [5] |
| | | 910 | 50 | [28] |
| | | 757 | 150 | [29] |
| | | 775 | 50 | [30] |
| | | 819 | 200 | [31] |
| | | 844 | 50 | [32] |
| | $Sn(C_2O_4)_2$ | 904 | 200 | [33] |
| | | 844 | 175 | [34] |
| | $Na_2SnO_3{\cdot}4H_2O$ | 1015 | 200 | [35] |
| | | 830 | 100 | [36] |
| Solvothermal | $SnCl_4$ | 1198 | 115 | [13] |
| | | 1015 | 100 | [37] |
| | | 1072 | 100 | [38] |
| | | 720 | 70 | [39] |
| | | 793 | 150 | [40] |
| Milling | Sn powder | 891 | 50 | [41] |
| | Nano-$SnO_2$ | 1351 | 40 | [42] |

Footnote: The potential range of the studies varied and some extended up to 3 V. We preferred to exhibit 100 mA $g^{-1}$ scan rate data but some of the capacities were obtained at slower scan rates.

starts from tin (II or IV) chlorides, or tin oxalate precursors and the most efficient electrodes are produced by hydrothermal or solvothermal processing. Thermal processing is much more economic than the vacuum deposition protocols, but it still requires heating of a large volume of dilute tin oxide dispersions in an autoclave. Ball milling was also successfully pursued, but it is economically inferior. Additionally, starting with chloride or oxalate salts produces large volume of acidic wastes that should be neutralized and safely discarded. Larcher and Tarascon[6] analyzed the sustainability of electric storage devices and concluded that low temperature processing and waste minimization increasingly determine electrode choice.

In this article we propose a new environmentally-friendly technique for the production of efficient tin oxide–graphene lithium ion battery anodes based on solution chemistry. The process starts from stannous hydroxide precursors, uses only aqueous hydrogen peroxide and alcohol as reagents, and the coating is accomplished at room temperature. Final heat treatment is therefore required only for the active material, which minimizes energy requirements and reactors costs. Hydrogen peroxide destruction does not generate waste and alcohol can be easily recycled, with no wastes generated in the process. In a previous article,[7] tetramethylammonium peroxostannate was deposited on graphene oxide, and converted by heat treatment to tin dioxide, methanol and trimethylamine. However, the amine and methanol are undesirable side products. Here, we show that reduced

graphene oxide - sodium stannates ($Na_xSnO_{2+x/2}$) can be used as efficient lithium ion battery anodes. Hydrogen peroxide is used in this protocol as a reagent and as a dispersion agent, and it prevents the rapid and uncontrolled tin oxide polycondensation and precipitation. As far as we know, sodium stannate was never used as lithium ion battery anode material.

## Experimental

**Materials and methods.**

**Preparation of graphene oxide.**

Graphene oxide (GO) was synthesized from exfoliated carbon by a modified Hummers method.[43,44] In a first step, graphite powder (1 g) was added to a solution of $K_2S_2O_8$ (1.67 g) and $P_2O_5$ (1.67 g) in 8 mL concentrated $H_2SO_4$. The mixture was kept at 80 °C for 4.5 h on a hot plate. After the mixture was cooled to room temperature, it was diluted with 0.35 L of deionized water (DIW) and filtered. Then, the preoxidized material was washed with DIW and dried at 60–70 °C overnight. In a second step, preoxidized carbon was redispersed in 40 mL of concentrated $H_2SO_4$, and the mixture was kept in an ice bath. Then, 5 g of $KMnO_4$ were added gradually under constant stirring to avoid overheating. The mixture was stirred at 35 °C for 2 h, and then slowly diluted with 80 mL of DIW upon cooling in the ice bath. The mixture was stirred for an additional 2 h, and then an additional 250 mL of DIW was added, followed by addition of 6 mL of 30 % $H_2O_2$ to react with the excess permanganate. The color of the solution changed to yellow after addition of the peroxide. The oxidized product was filtered and washed with 100 mL HCl (1:10) to remove metal ion impurities, followed by washing with 300 ml of DIW to remove the acid. A dispersion of GO in water was prepared by dispersing the oxidized material in DIW in an ultrasonic bath for 2 h.

**GO supported Sodium Peroxostannate.**

373 mg of $Na_2Sn(OH)_6$ (supplied by Sigma-Aldrich as sodium stannate trihydrate) were dissolved in 10 mL of aqueous $H_2O_2$ (17 %). Typically, 3.8 g of aqueous GO dispersion (1.5 %wt.) were dispersed in 20 mL of hydrogen peroxide (17 %) by sonication. Afterwards, peroxostannate solution was added into the GO dispersion. Precipitation of peroxostannate onto the GO surface was accomplished by addition of 50 mL ethanol. The coated GO was washed few times with the ethanol and dried under vacuum at room temperature. The coated material denoted here is as NaSnOx-GORT was stored in a 4°C refrigerator.

The samples NaSnOx-GO250, NaSnOx-GO400, NaSnOx-GO500-1, NaSnOx-GO500-2 were prepared from NaSnOx-GORT powder by heat treatment in vacuum at 250 °C for 3 h, 400 °C for 2 h, and 500 °C for 1 h and 2 h, respectively. The furnace temperature was raised from room temperature to the set point at a rate of 0.8 °C $min^{-1}$.

**Tetramethylammonium peroxostannate coated GO.**

The material was prepared according to a protocol that was described before.[7] First, the hydroxostannate precursor solution was prepared. 10 mL of $SnCl_4$ (0.086 mol) was dissolved in a few mL of DIW and neutralized with ammonia to pH 7. The precipitate was washed several times with DIW and dissolved in 31 mL of 25 % aqueous tetramethylammonium hydroxide (0.086 mol). After full dissolution, DIW was added to achieve a 1.4 M tin. 2.8 g of aqueous GO dispersion (2 wt%) were dispersed in 15 mL of hydrogen peroxide (30 %) by sonication. Then, 0.7 mL of hydroxostannate solution (1.4 M) was added. Precipitation of peroxostannate onto the GO surface was accomplished by addition of 80 mL of ethyl alcohol. The coated GO was washed with ethyl alcohol and subsequently with diethyl ether and dried under vacuum at room temperature. The coated material was heated under vacuum to 500 °C and is denoted here as $SnO_2$-GO.

**Active oxygen determination.**

Peroxostannate coated graphenes were dried at room temperature under vacuum. 50 mg of the dried material was redispersed in an acid mixture, which was prepared by dilution of 1 mL of concentrated $H_2SO_4$ with 4 mL of DIW and then mixed with 5 mL of saturated boric acid solution. The dispersion was stirred for 20 h and then filtered to remove the graphenes. The hydrogen peroxide that was released by the acid was determined by permanganometric titration with 0.03 N $KMnO_4$.[45]

**Electrochemical measurements.**

Samples NaSnOx-GO250, NaSnOx-GO400, NaSnOx-GO500-1, NaSnOx-GO500-2 where tested as active anode material. 60 wt% of the coated rGO, 20 wt% acetylene black (Super-P), and 20 wt% carboxymethyl cellulose (CMC) binder were mixed into a 2:1 methanol:water solution. In view of a comment raised by an anonymous reviewer, we have conducted a set of tests using i) 90% active material and 10% CMC without adding carbon; ii) 80% active material 10% CMC and 10% acetylene black; and iii) 80% active material and 20% CMC binder. The same active material (NaSnOx-GO400) was used in all tests. The rate dependent charging capacities of the different electrodes were added in the ESI (Fig. S4). The electrode with 10% CMC and 10% CMC binder gave somewhat lower performance compared to the 60:20:20 composition, but the difference was within our inter-electrode variability. The electrodes without added carbon gave much inferior results compared to the 80:10:10 composition. The obtained slurry was coated onto Cu foil disks to form working electrodes, which were then dried in vacuum at 50 °C for 12 h to remove the solvent. Electrochemical measurement was carried out on the CR2016 coin cells with lithium metal as the counter/reference electrode, Whatman GF/F glass microfiber separator, and 1 M $LiPF_6$ in ethylene carbonate (EC)/diethyl carbonate (DEC) (1:1 by volume) electrolyte. 2 % v/v 4-Fluoro-1,3-dioxolan-2-one (FEC) was added to electrolyte mixtures to improve solid electrolyte interface (SEI) stability.

The coin cells were assembled in an Ar-filled glovebox with concentrations of moisture and oxygen below 1.0 ppm.

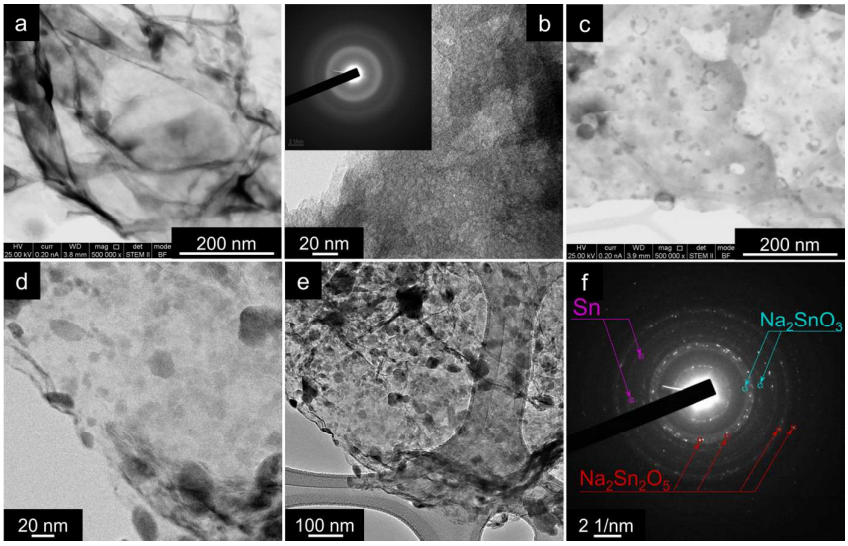


**Fig. 1** STEM and TEM images of graphene oxide supported sodium peroxostannate. a) STEM image of room graphene oxide supported peroxostannate before heat treatment, NaSnOx-GORT ; b) TEM image after heat-treatment at 250 °C, NaSnOx-GO250. Insert depicts the respective SAED; c) STEM image after heat treatment at 400 °C, NaSnOx-GO400; d,e) TEM image after heat treatment at 500 °C for 2h, NaSnOx-GO500-2. f) SAED of NaSnOx-GO500-2.

The charge/discharge tests were performed with a NEWARE battery tester at a voltage window of 0.01–2.5 V. Cyclic voltammetry (0.01–2.53 V, 0.1 mV $s^{-1}$) was performed with a Biologic VMP3 potentiostat. Details of TEM, SEM, STEM, XPS and XRD characterization procedures are provided in ESI.

## Results and Discussion

### Material characterization

We prepared four types of stannate supported graphene oxide. NaSnOx-GORT, peroxostannate supported GO, is the first coated product. It is received by wet chemistry at room temperature, and it serves as the precursor for the preparation of all other electrodes. NaSnOx-GO250 was formed after peroxide decomposition and sodium stannate formation at 250 °C. An analogous potassium precursor without graphenes was described in our previous publication.[46] NaSnOx-GO400 and NaSnOx-GO500-1 were obtained after heat treatment at 400 and 500 °C for 1 h. NaSnOx-GO500-2 was formed after heat treatment at 500 °C for 2 h. Additionally, we refer for comparison to $SnO_2$-GO, rGO supported tin oxide which was prepared from tetramethylammonium stannate precursor and discussed in ref.[7]

The preparation and characterization of sols of potassium peroxostannate and films of tetramethylammonium peroxostannate are documented elsewhere[7] and therefore we restrict the current description to those characteristics that illuminate the differences between the structural characteristics of the sodium stannate supported graphenes and the previously introduced tin oxide supported graphenes. Although the precursors of the two lines of materials are similar, the fact that the tetramethylammonium moiety disintegrates by thermal treatment endows the end materials with different morphological characteristics, and the presence of sodium provided somewhat different electrochemistry as well.

### Characteristics of the electrode materials

STEM studies of NaSnOx-GORT reveals featureless uniform coating of the graphene oxide (Fig. 1a). Permanganometric titration demonstrated that the material contained 4.2 wt% of peroxide. XRD studies (Fig. 2, curve 1) confirmed that the material is amorphous, and XPS study revealed that the Na:Sn in the amorphous material is close to 1 (Table 2, column 7). Heat treatment to 250 °C did not alter the morphology of the stannate as shown in Fig. 1b. The XRD study (Fig. 2, curve 2) confirmed that the material was amorphous after the 250 °C treatment. The two diffraction rings shown in the inserts of Fig. 1b with d-spacings of 0.21 and 0.12 $nm^{-1}$ are attributed to the graphene oxide support. Even after heat treatment at 400 °C the material retained its amorphous nature as can be readily seen in Fig. 1c and its SAED insert, as well as in the XRD diffractogram in Fig. 2 (curve 3). However, after 400 °C heat treatment the morphology of the material has changed and some circular features appeared (some marked by red circles in Fig. 1c). We attribute these circles to the gaseous emissions due to water evolution. Oxygen evolution due to peroxide disintegration could not be responsible for these bubble irruptions, since the thermal analysis (Fig. S1 in the ESI) shows that the exothermic peak of peroxide decomposition ends before 250 °C and the circular features do not appear at the corresponding Fig. 1b. Differential scanning calorimetry reveals an exothermic peak of the peroxide decomposition which starts already at 50 °C superimposed on a large endothermic process, which is attributed to water evaporation.

Heat treatment at 500 °C (NaSnOx-GO500-2) resulted in substantial morphological changes. Grains of up to 20 nm appeared on the surface of the graphenes (Fig. 1d and 1e). Tetragonal Romarchite, SnO, hexagonal sodium tin oxide,

$Na_2SnO_3$ and $Na_2Sn_2O_5$ phase appeared in the XRD diffractogram (Fig. 2).

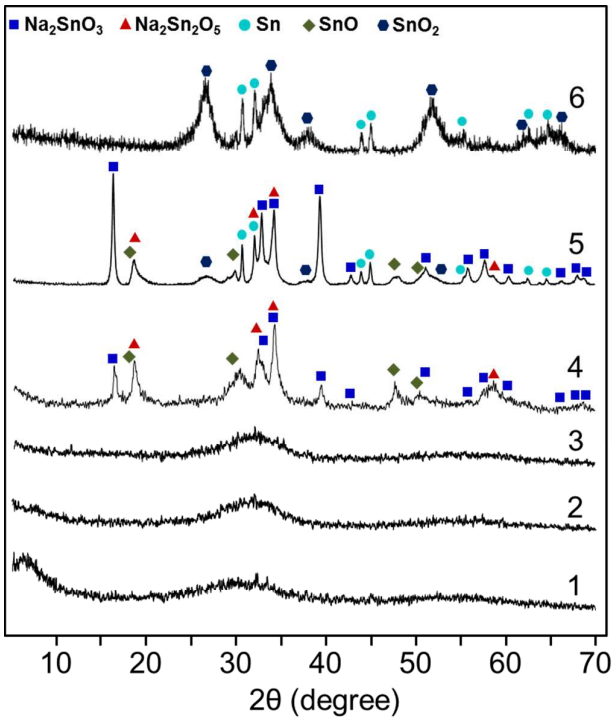


**Fig. 2** X-ray diffractograms of sodium stannate heat treated in vacuum at the indicated temperatures from bottom: (1) NaSnOx-GO RT, (2) NaSnOx-GO250, (3) NaSnOx-GO400, (4) NaSnOx-GO500-1,(5) NaSnOx-GO500-2, (6) $SnO_2$-GO. Major peaks of corresponding phases are denoted.

Heat treatment for 2 h at 500 °C resulted in the formation of tetragonal metallic tin (Sn(0)) with a crystalline size of 33 nm and crystals of $Na_2SnO_3$ of average size of 17 nm according to Scherrer equation. Additional minor phases of SnO and $SnO_2$ of 2 and 2.5 nm respectively could be discerned. The SAED analysis of NaSnOx-GO500-2 shows that the graphene rings with d-spacings of 0.21 and 0.12 $nm^{-1}$ were retained, and the diffraction spots of hexagonal sodium tin oxide, $Na_2SnO_3$ and $Na_2Sn_2O_5$ phase appeared. Detailed XRD data were added to the ESI (Fig. S2).

XPS studies (Fig. 3) help to glean insight on the mechanisms of the observed thermal transformations. The Sn 3d3/2 peak overlaps the Auger signal ($Na_{KLL}$), and therefore it is preferable to analyze the symmetric Sn 3d5/2 peak which remains at 486.7 up to 500°C. The small SnO phase that is observed in the XRD studies of NaSnOx-GO500-1 could not be seen, since it is practically impossible to resolve the 3d3/2 small peak of SnO from the large $Na_2SnO_3$ peak. The two peaks are broad, and are only 0.7 eV apart.[47,48] The additional Sn(0) peak at 485 eV appeared only after 2 hours of heat treatment at 500 °C, in agreement with the XRD studies. In a series of articles[7,49-51] we have demonstrated that the graphene support acts as a reducing agent at the thermal treatment of GO supported antimony and tin oxides.

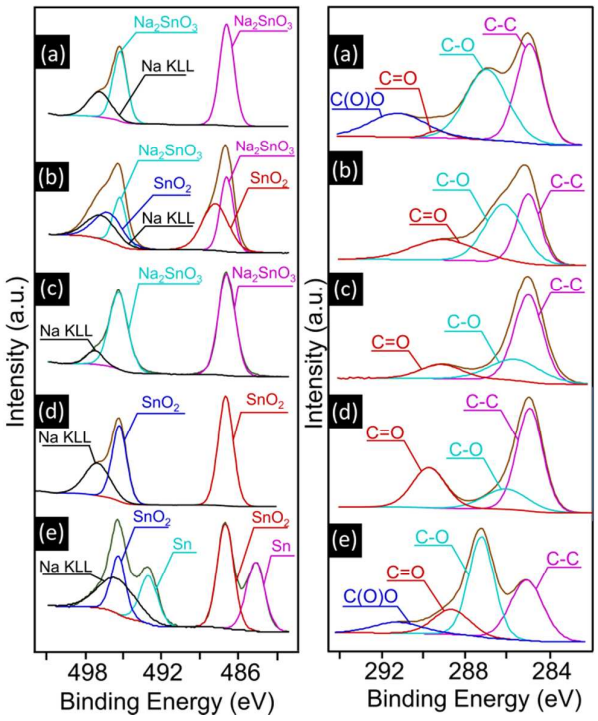


**Fig. 3** XPS studies of Sn 3d (left) and C1s. a) NaSnOx-GORT; b) NaSnOx-GO250; c) NaSnOx-GO400; d) NaSnOx-GO500-1; e) NaSnOx-GO500-2.

It is therefore informative to discern the changes in the XPS C 1s spectra of GO supported peroxostannate and stannate. Before heat treatment (upper curve of frame b in Fig. 4) the spectrum shows a peak of sp2 carbon at 284.8 eV, in accordance with previous observations,[51-53] and oxygenated carbon moieties: C–O (287 eV), carbonyls C=O (289.0 eV) and carboxylates COOH (291 eV). Although the assignment of these peaks can be argued, it is clear that the higher binding energy moieties (>287 eV) can be attributed to more oxygenated carbon atoms. As expected, up to 400 °C, heat treatment reduced the relative abundance of the oxygenated carbon peaks, and the center of gravity of the carbon binding energies shifted gradually to lower energies .Taking the room temperature as a baseline there was a shift of -0,32 eV and -0.34eV after treatment at 250 and 400 °C, respectively. However, after treatment for 1 h at 500 °C, with the appearance of the SnO phase in the x-ray diffractogram, the center of gravity of the binding energies of C 1s electrons shifted back to higher energies, +0.41 eV relative to the base line 286.09 eV indicating that the graphene support was oxidized. This oxidation process was further enhanced with the formation of the elemental tin phase after 2 h of heat treatment at 500 °C, and the center of gravity shifted by +0.92 eV relative to the baseline. Centers of gravity: NaSnOx-GORT - 286.09; NaSnOx-GO250 - 286,40; NaSnOx-GO400 - 285.75; NaSnOx-GO500-1 - 286.50; NaSnOx-GO500-2 - 287.01 eV.

We therefore believe that the changes in the XRD and XPS spectra as a function of the heat treatment allow us to glean the underlying transformations: Up to 400 °C, the GO is gradually reduced. Following short heat treatment at 500 °C,

the rGO is somewhat oxidized by the reduction of tin dioxide to tin monoxide. Longer thermal treatment reduces the tin oxide to elemental tin and the tin oxide almost disappears. Throughout these transformations the sodium stannate moieties remain stable, and they are not reduced by heat treatment despite the presence of the rGO reducing agent.

Table 2: Elemental composition of the anode materials.*

| Electrode material | Na | | Sn | | C | Na/Sn |
|---|---|---|---|---|---|---|
| | at, % | wt, % | at, % | wt, % | wt, % | at. |
| NaSnOx-GO-RT | 7.46 | 7.82 | 7.05 | 38.15 | 11.46 | 1.058 |
| NaSnOx-GO250 | 8.64 | 8.57 | 8.18 | 41.91 | 8.92 | 1.056 |
| NaSnOx-GO400 | 8.03 | 7.96 | 8.50 | 43.50 | 8.54 | 0.945 |
| NaSnOx-GO500-2 | 8.16 | 8.05 | 8.53 | 43.49 | 7.74 | 0.957 |
| NaSnOx-GO400 (after cycling) | 1.22 | 1.48 | 1.07 | 7.33 | | 1.14 |

Footnote: Na and Sn content were derived by XPS, C content derived by CHN analysis. The presence of the binder prevented C analysis of the EC tested electrode.

The thermal transformations of the GO supported sodium peroxostannate differ from the transformations of the GO coated tetramethylammonium peroxostannate (not shown here). The sodium stannate remained amorphous even after 400 °C, whereas partial decomposition of the tetramethylammonium peroxostannate occurred already at room temperature and some nanocrystalline cassiterite $SnO_2$ phase appeared according to the XRD. We attribute these differences to the larger stability of the sodium stannate compared to tetramethylammonium stannate. The tetramethylammonium moiety decomposed at low temperature (below 200 °C) and the resulting trimethylamine and methanol were evaporated during the vacuum heat treatment, whereas the sodium counter ion remained. Thus, the sodium interfered with the crystallization process, and it was delayed until 500 °C. At this high temperature, both SnO and sodium stannate appeared since the Na:Sn stoichiometry of the material is only 1:1 (Table 2). The SnO phase was produced by thermal reduction of $SnO_2$ by the graphene support. After still longer heat treatment at 500 °C the SnO phase was further reduced to Sn(0), stannates were not reduced by the graphenes. Two practical consequences thus distinguish the sodium stannate from the tetramethylammonium stannate transformations: i) sodium peroxostannate is stable at room temperature and does not produce toxic gases during the heat treatment; ii) Only amorphous phase was obtained at 400 °C for the sodium stannate electrode while the use of tetramethylammonium precursor results a crystalline product already at room temperature; and iii) additional crystalline phase, $Na_2SnO_3$ and $Na_2Sn_2O_5$ were formed from the sodium peroxostannate precursor. However, both pathways give Sn(0) phases after heat treatment at 500 °C.

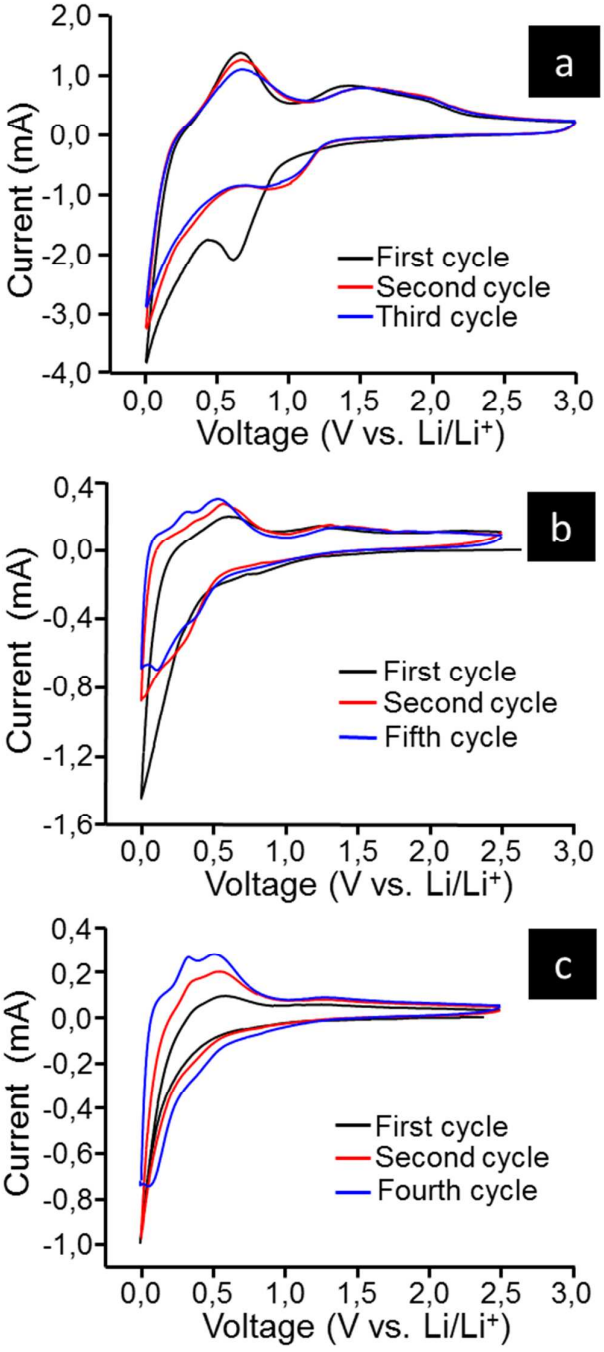


**Fig. 4** Cyclic voltammetry of $SnO_2$-GO (a), NaSnOx-GO400 (b) and NaSnOx-GO500-1 (c) after the indicated number of cycles at 0.1 mV/s scan rate.

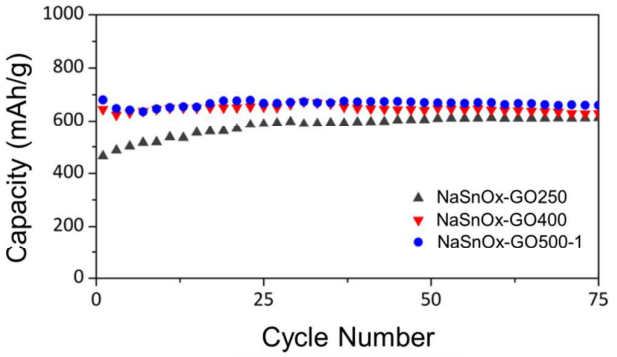


**Fig. 5** Charge capacity of the NaSnOx-GO250, NaSnOx-GO400, and NaSnOx-GO500-1 anodes upon repeated cycling. The cycles were conducted at a rate of 100 mA $g^{-1}$ between 0–2.5 V vs. $Li/Li^+$.

**Cyclic voltammetry studies**

The cyclic voltammetry studies of the $SnO_2$-GO, NaSnOx-GO400 and NaSnOx-GO500-1 are depicted in Fig. 4. The cathodic first scan of $SnO_2$-GO (Fig. 4a) exhibited a current peak at 0.7 V, and a monotonic current increase up to a maximum at the reversal point 0.05 V. The anodic scan exhibited two peaks at 0.6 and 1.3 V. The first pair of maxima at 0.05 and 0.6 V is due to the reversible alloying and de-alloying of Li-Sn, and there is indeed no substantial change of the positions and current of the anodic peak in subsequent cycles. The second pair of peaks (at 0.7-1, 1.30 V) is related to decomposition and reformation of $SnO_2$. Upon subsequent cycles the second cathodic peak shifted from 0.7 to ca 1. V and the broad 1.3 V peak remained almost at the same potential. The shift of the first cathodic peak from 0.7 to 1 V, upon cycling is attributed to the formation of solid electrolyte interface (SEI). The cyclic voltammetry of the NaSnOx-GO electrodes is similar (frames b,c), the reversible pair of maxima at near 0 V and 0.6 V appears as well as the more sluggish peaks at 1.2 V and at 0.8 V. However, there are also some differences. First, the more anodic pair of peaks is less pronounced showing that these electrodes can benefit less from the reversible formation of tin oxide (equation 1).

The anodic scans show that a peak at 0.35 V gradually develops during the first five cycles. Concurrent with the development of this anodic peak we witness the gradual formation of small peak at 0.004 V during the first few cycles. It is tempting to attribute this anodic peak to the de-alloying of the sodium-tin phase by the reversal of equation 3.

$$Sn + 3.75\ Li^+ + 3.75e^- = SnLi_{3.75} \quad (3)$$

However, sodium is reduced at 0.33 V more positive to lithium reduction, and therefore a peak at 0.35 vs $Li/Li^+$ (with a threshold at 0.15 V as observed in Fig. 4c) due to sodium-tin reductive de-alloying is not likely.

Sodium alloying in tin based batteries, such as Sn, SnSb, $SnS_2$ was amply researched.[55-60] These reports show an oxidation peak (or differential capacity peak) at 0.17 – 0.2 V vs. $Na/Na^+$ reference, corresponding to *ca* 0.5 V vs $Li/Li^+$ electrode. This peak coincides with the Li-tin de-alloying peak and could not be distinguished in our studies.

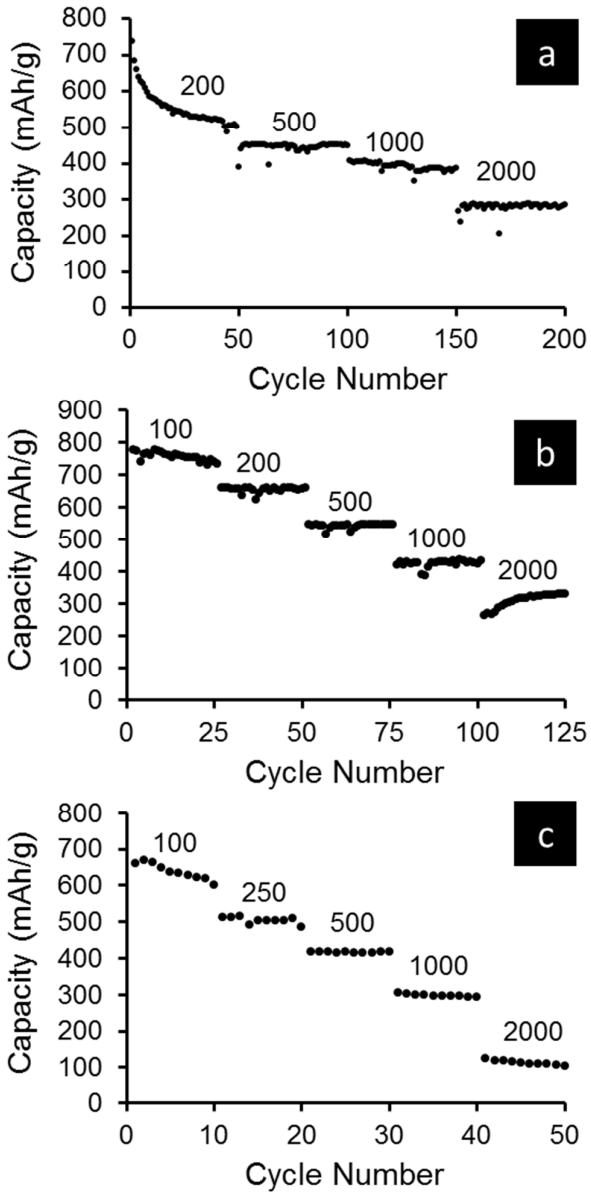


**Fig. 6** Charging capacities of the NaSnOx-GO250 (a), NaSnOx-GO400 (b), and NaSnOx-GO500-1 (c) anodes conducted over the range 0–2.5 V vs. Li/Li+ electrode at different rates.

Komaba et al.[61] showed that the addition of sodium cation to the electrolyte of a graphite lithium ion battery improves the performance of the anode. The improved performance was attributed to decreased interfacial resistance. However, since graphite cannot intercalate substantial amount of sodium, the analogy between tin alloying and graphite intercalation is of limited mechanistic

consequences. Therefore, we attribute the peak at 0.35 vs $Li/Li^+$ to the de-alloying of a ternary sodium–lithium-tin alloy that is formed at cathodic wave (0.5-0 V). The fact that a ternary phase is involved, may also explain the delayed appearance of this phase, which gradually appeared only after several cycles. We have carried out EDX studies of the cycled electrode, and Table 2 shows that the Na:Sn ratio in the electrode was not altered by the cycling and the sodium is retained on the electrode. Thus sodium alloying can take place even after many cycles, which provides a simple explanation for the 0.35V anodic peak.

NaSnOx-GO400 showed the best capacity retention among the tested electrodes (Fig. 5) though the other electrode materials exhibited almost equally good performance at low charging rates. A charge capacity of about 610 mAh $g^{-1}$ was maintained for cycles at a rate of 100 mA h $g^{-1}$ after 140 cycles (shown only as Fig. S3 in the ESI). We attribute the improved performance of the NaSnOx-GO400 to higher conductivity due to the higher degree of graphene oxide reduction compared to the samples that were heat treated at 250 °C. In addition, the NaSnOx-GO400 sample was amorphous and therefore exhibited better performance compared to the crystalline and less accessible phases that were formed at 500 °C. This behavior differs from the $SnO_2$-GO electrodes which were reported before[7] and exhibited best performance only after heat treatment at 500 °C and crystalline phase formation.

Rate performance was performed for the NaSnOx-GO400 anode conducted over the range 0–2.5 V *vs.* $Li/Li^+$ electrode. 400 and 315 mAh $g^{-1}$ were obtained even at 1000 and 2000 $mAg^{-1}$ and extended period of cycling (Fig. 6). Interestingly the NaSnOx-GO250 which is also amorphous exhibited also a very good performance of 300 mAh $g^{-1}$ at 2000 $mAg^{-1}$, remarkably superior to the more crystalline NaSnOx-GO500-1 electrode that was prepared at 500 °C.

SEM studies of the cycled electrodes confirmed absence of dendrite formation by repeated cycling, a prerequisite of a lithium ion battery anode (Fig. S5).

## Conclusions

The graphene oxide supported sodium stannate electrode which was introduced in this study provides a different, more environmentally friendly route to tin based anode preparation. Though its theoretical and practical charge capacity performance is somewhat inferior to some of the more recently introduced active anode material its manufacturing process compensates for this drawback. The production process does not involve acidic wastes and the only solvent that is used, ethanol is cheap and can be conveniently recycled in the process. Energy demanding processing such as solvothermal, hydrothermal and balls milling are not required and the thermal treatment of the solid at 400 °C can be done in a relatively small, cheap and at low pressure reactors.

## Acknowledgements

This research is supported by the Singapore National Research Foundation under CREATE programmes: TUM CREATE Centre for Electromobility and Nanomaterials for Energy and Water Management by the Israel Ministry of Science and the Energy Research Institute at Nanyang Technological University. We thank The Harvey M. Krueger Family Center for Nanoscience and Nanotechnology of the Hebrew University of Jerusalem and the Israel Science Foundation and I-SAEF, Israel Strategic Alternative Energy Foundation, for financial support. We thank the Russian Foundation for Basic Research (grant 14-29-04074), the Council on Grants of the President of the Russian Federation (MK-5847.2014.3, SP-995.2015.1), the Target Programs for Basic Research of the Presidium of the Russian Academy of Sciences and the Division of Chemistry and Materials Science of the Russian Academy of Sciences. A.G. Medvedev and A.A. Mikhaylov thankfully acknowledge a Golda Meir and Vallazzi-Pikovsky Postdoctoral Fellowships for support. C.W. Mason thanks Heryani Bin Ahmad and Felix Lange for assistance in carrying out electrochemical evaluations.

## References

1 H. Buqa, D. Goers, M. Holzapfel, M. E. Spahr and P. Novák, *J. Electrochem. Soc.*, 2005, **152**, A474-A481.
2 J. Y. Huang, L. Zhong, C. M. Wang, J. P. Sullivan, W. Xu, L. Q. Zhang, S. X. Mao, N. S. Hudak, X. H. Liu, A. Subramanian, H. Fan, L. Qi, A. Kushima and J. Li, *Science*, 2010, **330**, 1515-1520.
3 R. Wang, C. Xu, J. Sun, L. Gao and H. Yao, *ACS Appl. Mater. Interfaces*, 2014, **6**, 3427-3436.
4 Q. Guo, Z. Zheng, H. Gao, J. Ma and X. Qin, *J. Power Sources*, 2013, **240**, 149-154.
5 D. Wang, J. Yang, X. Li, D. Geng, R. Li, M. Cai, T. Sham and X. Sun, *Energy Environ. Sci.*, 2013, **6**, 2900-2906.
6 D. Larcher and J. M. Tarascon, *Nat Chem*, 2015, **7**, 19-29.
7 S. Sladkevich, J. Gun, P. V. Prikhodchenko, V. Gutkin, A. A. Mikhaylov, V. M. Novotortsev, J. X. Zhu, D. Yang, H. H. Hng, Y. Y. Tay, Z. Tsakadze and O. Lev, *Nanotechnology*, 2012, **23**, 485601.
8 J. Cheng, H. Xin, H. Zheng and B. Wang, *J. Power Sources*, 2013, **232**, 152-158.
9 J. Guo, B. Jiang, X. Zhang and H. Liu, *J. Power Sources*, 2014, **262**, 15-22.
10 Q. Guo, S. Chen and X. Qin, *Mater. Lett.*, 2014, **119**, 4-7.
11 Q. Guo, S. Chen and X. Qin, *Mater. Lett.*, 2014, **128**, 50-53.
12 N. Li, H. Sonsg, H. Cui and C. Wang, *Electrochim. Acta*, 2014, **130**, 670-678.
13 P. Lian, S. Liang, X. Zhu, W. Yang and H. Wang, *Electrochim. Acta*, 2011, **58**, 81-88.
14 H. Liu, J. Huang, X. Li, J. Liu, Y. Zhang and K. Du, *Appl. Surf. Sci.*, 2012, **258**, 4917-4921.
15 X. Liu, J. Cheng, W. Li, X. Zhong, Z. Yang, L. Gu and Y. Yu, *Nanoscale*, 2014, **6**, 7817-7822.
16 C. Xu, J. Sun and L. Gao, *Nanoscale*, 2012, **4**, 5425-5430.
17 C. Xu, J. Sun and L. Gao, *J. Mater. Chem.*, 2012, **22**, 975-979.
18 S. Yang, W. Yue, J. Zhu, Y. Ren and X. Yang, *Adv. Funct. Mater.*, 2013, **23**, 3570-3576.
19 X. Zhou, L. Wan and Y. Guo, *Adv. Mater.*, 2013, **25**, 2152-2157.
20 C. Tan, J. Cao, A. M. Khattak, F. Cai, B. Jiang, G. Yang and S. Hu, *J. Power Sources*, 2014, **270**, 28-33.

21 J. Zhang, L. Chang, F. Wang, D. Xie, Q. Su, G. Du, *Mater. Res. Bull.,* 2015, **68**, 120-125.
22 Q. Guo and X. Qin, *Ecs Solid State Lett.*, 2013, **2**, M41-M43.
23 B. Huang, J. Yang, Y. Zou, L. Ma and X. Zhou, *Electrochim. Acta*, 2014, **143**, 63-69.
24 L. Li, A. Kovalchuk and J. Tour, *Nano Res.*, 2014, **7**, 1319-1326.
25 J. Lin, Z. Peng, C. Xiang, G. Ruan, Z. Yan, D. Natelson and J. Tour, *Acs Nano*, 2013, **7**, 6001-6006.
26 H. Lu, N. Li, M. Zheng, L. Qiu, S. Zhang, J. Zheng, G. Ji and J. Cao, *Mater. Lett.*, 2014, **115**, 125-128.
27 B. Vinayan and S. Ramaprabhu, *J. Mater. Chem. A*, 2013, **1**, 3865-3871.
28 X. Wang, X. Cao, L. Bourgeois, H. Guan, S. Chen, Y. Zhong, D. Tang, H. Li, T. Zhai, L. Li, Y. Bando and D. Golberg, *Adv. Funct. Mater.*, 2012, **22**, 2682-2690.
29 C. Zhang, X. Peng, Z. Guo, C. Cai, Z. Chen, D. Wexler, S. Li and H. Liu, *Carbon*, 2012, **50**, 1897-1903.
30 B. Zhao, G. Zhang, J. Song, Y. Jiang, H. Zhuang, P. Liu and T. Fang, *Electrochi. Acta*, 2011, **56**, 7340-7346.
31 J. Zhu, D. Wang, L. Wang, X. Lang and W. You, *Electrochim. Acta*, 2013, **91**, 323-329.
32 D. Cai, T. Yang, B. Liu, D. Wang, Y. Liu, L. Wang, Q. Li and T. Wang, *J. Mater. Chem. A*, 2014, **2**, 13990-13995.
33 B. Chen, H. Qian, J. Xu, L. Qin, Q. Wu, M. Zheng and Q. Dong, *J. Mater. Chem. A*, 2014, **2**, 9345-9352.
34 S. M. Lee, S. H. Choi and Y. C. Kang, *Chem. – Eur. J.*, 2014, **20**, 15203-15207.
35 S. Liu, R. Wang, M. Liu, J. Luo, X. Jin, J. Sun and L. Gao, *J. Mater. Chem. A*, 2014, **2**, 4598-4604.
36 X. Zhou, W. Liu, X. Yu, Y. Liu, Y. Fang, S. Klankowski, Y. Yang, J. Brown and J. Li, *ACS Appl. Mater. Interfac.*, 2014, **6**, 7434-7443.
37 P. Lian, J. Wang, D. Cai, L. Ding, Q. Jia and H. Wang, *Electrochim. Acta*, 2014, **116**, 103-110.
38 P. Lian, X. Zhu, S. Liang, Z. Li, W. Yang and H. Wang, *Electrochim. Acta*, 2011, **56**, 4532-4539.
39 Z. Li, G. Wu, D. Liu, W. Wu, B. Jiang, J. Zheng, Y. Li, J. Li and M. Wu, *J. Mater. Chem. A*, 2014, **2**, 7471-7477.
40 X. Li, X. Meng, J. Liu, D. Geng, Y. Zhang, M. Banis, Y. Li, J. Yang, R. Li, X. Sun, M. Cai and M. Verbrugge, *Adv. Funct. Mater.*, 2012, **22**, 1647-1654.
41 F. Ye, B. Zhao, R. Ran and Z. Shao, *Chem.- Eur. J.*, 2014, **20**, 4055-4063.
42 Z. Chen, M. Zhou, Y. Cao, X. Ai, H. Yang and J. Liu, *Adv. Energy Mater.*, 2012, **2**, 95-102.
43 W. S. Hummers and R. E. Offeman, *J. Am. Chem. Soc.*, 1958, **80**, 1339-1339.
44 Y. X. Xu, H. Bai, G. W. Lu, C. Li and G. Q. Shi, *J. Am. Chem. Soc.*, 2008, **130**, 5856-5857.
45 W. C. Schumb, C. H. Satterfield and R. L. Wentworth, *Hydrogen peroxide*, Reinhold Publishing Corporation, New York, 1955.
46 S. Sladkevich, V. Gutkin, O. Lev, E. A. Legurova, D. F. Khabibulin, M. A. Fedotov, V. Uvarov, T. A. Tripol'skaya and P. V. Prikhodchenko, *J. Sol Gel Sci. Technol.*, 2009, **50**, 229-240.
47 F. Akgul, C. Gumus, A. Er, A. Farha, G. Akgul, Y. Ufuktepe and Z. Liu, *J. Alloys Compd.*, 2013, **579**, 50-56.
48 X-ray photoelectron spectroscopy (XPS) reference pages, http://www.xpsfitting.com, (accesed January 2015).
49 S. Sladkevich, J. Gun, P. V. Prikhodchenko, V. Gutkin, A. A. Mikhaylov, A. G. Medvedev, T. A. Tripol'skaya and O. Lev, *Carbon*, 2012, **50**, 5463-5471.
50 P. V. Prikhodchenko, J. Gun, S. Sladkevich, A. A. Mikhaylov, O. Lev, Y. Y. Tay, S. K. Batabyal and D. Y. W. Yu, *Chem. Mater.*, 2012, **24**, 4750-4757.
51 D. Y. W. Yu, P. V. Prikhodchenko, C. W. Mason, S. K. Batabyal, J. Gun, S. Sladkevich, A. G. Medvedev and O. Lev, *Nat. Commun.*, 2013, **4**, 2922.
52 I. K. Moon, J. Lee, R. S. Ruoff and H. Lee, *Nat. Commun.*, 2010, **1**, 73.
53 S. Stankovich, D. A. Dikin, R. D. Piner, K. A. Kohlhaas, A. Kleinhammes, Y. Jia, Y. Wu, S. T. Nguyen and R. S. Ruoff, *Carbon*, 2007, **45**, 1558-1565.
54 54.D. Yang, A. Velamakanni, G. Bozoklu, S. Park, M. Stoller, R. D. Piner, S. Stankovich, I. Jung, D. A. Field, C. A. Ventrice Jr and R. S. Ruoff, *Carbon*, 2009, **47**, 145-152.
55 55.S. Komaba, Y. Matsuura, T. Ishikawa, N. Yabuuchi, W. Murata and S. Kuze, *Electrochem. Commun.*, 2012, **21**, 65-68.
56 M. K. Datta, R. Epur, P. Saha, K. Kadakia, S. K. Park and P. N. Kuma, *J. Power Sources*, 2013, **225**, 316-322.
57 L. F. Xiao, Y. L. Cao, J. Xiao, W. Wang, L. Kovarik, Z. M. Nie and J. Liu, *Chem. Commun.*, 2012, **48**, 3321-3323.
58 K. Chang, Z. Wang, G. C. Huang, H. Li, W. X. Chen and J. Y. Lee, *J. Power Sources*, 2012, **201**, 259-266.
59 S. Y. Liu, X. Lu, J. Xie, G. S. Cao, T. J. Zhu and X. B. Zhao, *Acs Appl. Mater. Interf.*, 2013, **5**, 1588-1595.
60 B. Luo, Y. Fang, B. Wang, J. S. Zhou, H. H. Song and L. J. Zhi, *Energy Environ. Sci.*, 2012, **5**, 5226-5230.
61 S. Komaba, T. Itabashi, B. Kaplan, H. Groult and N. Kumagai, *Electrochem. Commun.*, 2003, **5**, 962-966.